



On the electronic structure and chemical bonding of titanium tetraauride: TiAu_4 and TiAu_4^-

Yusuf Erdogan^{a,b}, Tian Jian^b, Gary V. Lopez^b, Wei-Li Li^b, Lai-Sheng Wang^{b,*}

^a Department of Physics, Ahi Evran University, Kirsehir 40100, Turkey

^b Department of Chemistry, Brown University, Providence, RI 02912, USA



ARTICLE INFO

Article history:

Received 13 May 2014

In final form 8 July 2014

Available online 14 July 2014

ABSTRACT

The structural and electronic properties of titanium tetraauride are investigated using photoelectron spectroscopy and density functional calculations. The photoelectron spectra of TiAu_4^- show a relatively simple spectral pattern with a large energy gap, suggesting that neutral TiAu_4 has a highly stable electronic configuration. Theoretical calculations have found a slightly distorted tetrahedral structure for TiAu_4^- , whereas the closed shell neutral TiAu_4 has perfect T_d symmetry. Chemical bonding analyses suggest that the Au–Ti bonds have multiple bond characters due to the Au 5d to Ti 3d back donation and that chemical bonding in the tetraauride is similar to that in heavier titanium tetrahalides.

© 2014 Elsevier B.V. All rights reserved.

1. Introduction

Gold exhibits many unusual properties derived from the strong relativistic effects [1–3] that stabilize the outer 6s shell and destabilize the 5d shell, including significant s-d hybridization and capacities to form strong covalent bonds [4]. Hence, Au has the highest electron affinity (EA) (2.309 eV) and simultaneously the highest ionization potential (9.225 eV) among all the metal elements. On the Pauling scale, the electronegativity of gold is also the highest among the metallic elements. Thus, even though gold is a metallic element, it can also act as an electron acceptor to form a stable auride anion, such as in the ionic compound CsAu [1]. The high electronegativity of gold is also manifested by its similar chemical properties to the heavier halides, such as Br and I [5–7]. The gold–halogen analogy has been examined in a previous theoretical study of metal tetraaurides MAu_4 ($\text{M} = \text{Ti}, \text{Zr}$ or Hf), which were predicted to have closed-shell tetrahedral (T_d) structures, similar to TiCl_4 [5]. However, this theoretical prediction has not been verified experimentally. Photoelectron spectroscopy (PES) combined with ab initio studies have shown that a single gold atom can also exhibit chemistry analogous to the hydrogen atom, such as SiAu_4 , which also adopts a T_d structure similar to SiH_4 [8]. The gold–hydrogen analogy has been found in many auride clusters of Si and B [9–14]. The strong covalent bond character observed in these auride clusters provides convincing evidence for the gold–hydrogen analogy.

An interesting question is, does Au behave more like a halogen or hydrogen when bonded to a transition metal atom?

Transition-metal (TM) doped noble metal alloy clusters constitute an active field of research because of their potential applications in nanoalloy catalysts and nanoelectronic devices [15–25]. There have also been numerous studies of doped gold clusters with main group elements [26–33]. However, to the best of our knowledge, there have been no experimental studies on Ti-doped gold clusters. In the current work, we report a combined PES and density functional theory (DFT) study of the anionic and neutral titanium tetraauride clusters. Our goal is to elucidate their structures and the nature of the chemical bond between Ti and Au. Our global minimum searches lead to a T_d structure for neutral TiAu_4 . However, the TiAu_4^- anion has a slightly distorted tetrahedral structure due to the Jahn–Teller effect. Photoelectron spectra reveal a large energy gap and confirm the tetrahedral structures for the titanium tetraauride. Chemical bonding analyses suggest that there are multiple bond characters in the Au–Ti bonds and that the Au–Ti bonding is similar to that in heavier titanium tetrahalides.

2. Experimental and theoretical methods

2.1. Photoelectron spectroscopy

The experiment was carried out using a magnetic-bottle PES apparatus equipped with a laser vaporization cluster source, details of which were published elsewhere [34]. Briefly, the TiAu_4^- cluster was produced by laser vaporization of a composite disk target made of Au and Ti (5 wt.%). Clusters formed in the source were

* Corresponding author.

E-mail address: lai-sheng.wang@brown.edu (L.-S. Wang).

entrained by He carrier gas and underwent supersonic expansion to from a collimated cluster beam. The He carrier gas was seeded with 5% Ar to achieve better supersonic cooling [35]. The cluster anions were extracted from the cluster beam and analyzed using a time-of-flight mass spectrometer. The TiAu_4^- cluster was mass-selected and decelerated before being photodetached. Three detachment photon energies were used in the current study: 355 nm (3.496 eV) and 266 nm (4.661 eV) from a Nd:YAG laser and 193 nm (6.424 eV) from an ArF excimer laser. Photoelectrons were collected at nearly 100% efficiency by the magnetic bottle and analyzed in a 3.5 m long electron flight tube. The PES spectra were calibrated using the known spectra of Bi^- and Au^- , and the energy resolution of the apparatus was $\Delta E_k/E_k \approx 2.5\%$, that is, ~ 25 meV for electrons with 1 eV kinetic energy.

2.2. Computational methods

The DFT structural searches for the anionic and neutral clusters were performed using the coalescence kick (CK) global minimum search program [36] at the B3LYP/LANL2DZ level of theory [37]. The low-lying candidate structures were then reoptimized at the B3LYP/Stuttgart (SDD) and PBEPBE/SDD [38] levels. Frequency calculations were done to confirm that the reported structures are true minima. The VDEs were computed using two methods: (1) Δ SCF-TDDFT [16,39]. In this approach, the ground-state energies of the anions and the neutrals were calculated at the optimized geometries of the anions from the Δ SCF energy differences, whereas the vertical excited-state energies of the electron-detached neutral species were obtained from TDDFT calculations at the geometries of the anions. These excitation energies were then added to the first VDE to approximate the high-lying VDEs. Only those neutral excited states with one-electron detachment from the anion ground state were chosen. (2) Δ SCF. The TDDFT cannot calculate the accurate excitation energy of the triplet excited states for TiAu_4 due to the orbital degeneracy lifted by uneven occupancy of the degenerate orbitals. The triplet final VDEs are thus calculated as the Δ SCF energy differences by defining the exact final electronic states at the anion geometry [40,41]. Both methods are done using B3LYP/SDD and B3LYP/Ti/Aug-cc-pVTZ/Au/Aug-cc-pVTZ-pp levels of theory [42,43]. Natural bond orbital (NBO) [44] analyses were performed on the optimized neutral geometry at B3LYP/SDD level of theory. These calculations were done using GAUSSIAN 09 [45].

3. Results and discussion

3.1. Experimental results

The photoelectron spectra measured at the three photon energies are displayed in Figure 1. The observed detachment transitions are labeled with X, A, B, ..., where band X represents electron detachment from the anion to produce the neutral electronic ground state. The higher binding energy bands (A, B, ...) denote detachment transitions to excited states of neutral TiAu_4 . The vertical detachment energies (VDEs) of all the observed bands are given in Table 1, where they are compared with the theoretical results.

The 193 nm spectrum (Figure 1c) reveals a large gap between bands X and A. The VDE of band X is measured to be 2.91 eV, whereas the VDE of the A band is 4.42 eV. The large energy gap of 1.51 eV between bands X and A indicates a large gap between the highest occupied (HOMO) and lowest unoccupied (LUMO) molecular orbitals of the neutral species, suggesting that TiAu_4 is a highly stable and closed-shell system. Two intense bands B (VDE: 4.63 eV) and C (VDE: 4.72 eV) are closely spaced with band A. Following another energy gap, two relatively weak features D (VDE: 6.00 eV) and E (VDE: 6.20 eV) are observed in the high binding energy region.

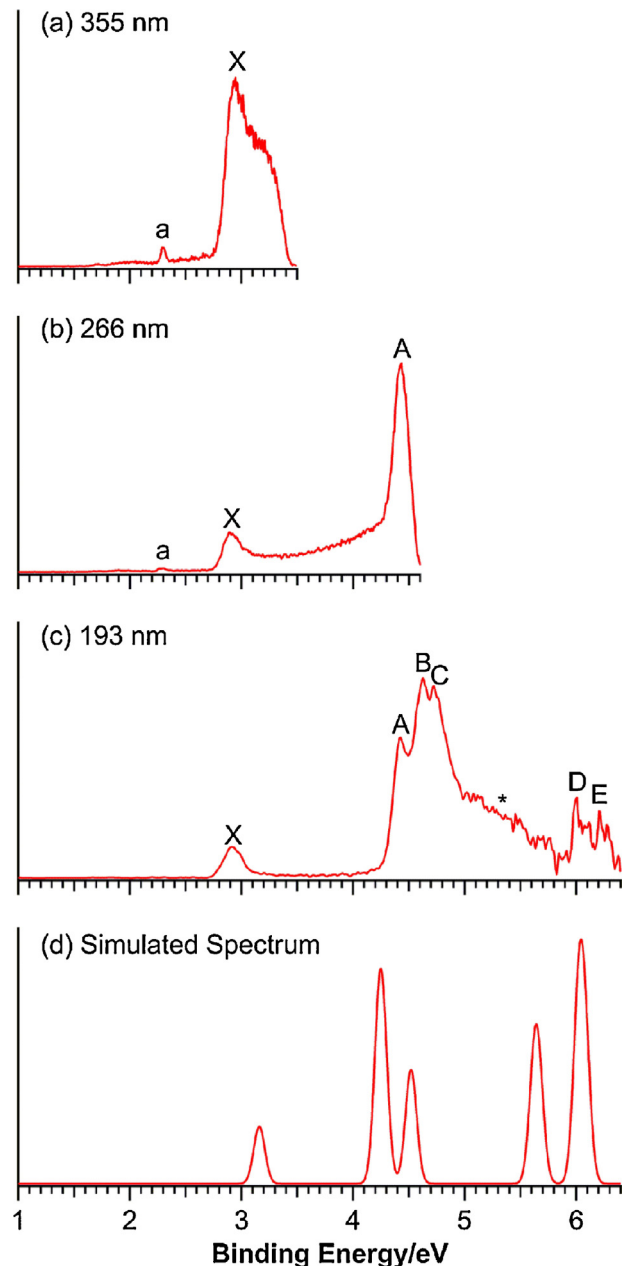


Figure 1. Photoelectron spectra of TiAu_4^- at (a) 355 nm, (b) 266 nm, (c) 193 nm, in comparison with the simulated spectrum (d) for the global minimum D_{2d} TiAu_4^- at B3LYP/SDD level. The simulated spectrum was obtained by fitting the calculated VDEs with a unit area Gaussian function of 0.12 eV full width at half maximum.

Some broad and continuous signals (*) are observed between 5 and 6 eV in the 193 nm spectrum. As will be shown later when compared to the theoretical results, these signals do not correspond to any direct one-electron detachment processes. They are likely due to indirect processes, either via shake-up or autodetachment processes [46].

We expected to obtain better-resolved spectra at lower photon energies. However, the 266 nm spectrum (Figure 1b) shows surprisingly relatively strong and continuous signals in the X and A band gap region. These continuous signals are reminiscent of thermionic emissions [47,48] i.e., the anion absorbs a 266 nm photon, which is rapidly converted to internal energies to create ‘superhot’ anions. These superhot anions can ‘boil’ off electrons, giving rise to the continuous signals, and also undergo fragmentation. The latter is evidenced by the observation of a very sharp peak labeled as

Table 1

Comparison of the experimental vertical detachment energies (VDEs) with the calculated values of TiAu_4^- (D_{2d} , $^2\text{B}_1$). All energies are in eV.

Features	VDE (expt.) ^a	Final states and their electronic configurations	VDE (theo.)		
X	2.91 (5)	$^1\text{A}_1, \dots 4\text{e}^4 3\text{a}_1^2 2\text{b}_1^2 5\text{e}^4 2\text{a}_2^2 4\text{a}_1^2 4\text{b}_2^2 6\text{e}^4 3\text{b}_1^0$	3.16 ^b	3.02 ^c	3.02 ^d
A	4.42 (6)	$^3\text{E}, \dots 4\text{e}^4 3\text{a}_1^2 2\text{b}_1^2 5\text{e}^4 2\text{a}_2^2 4\text{a}_1^2 4\text{b}_2^2 6\text{e}^3 3\text{b}_1^1$	4.21	4.18	4.18
B	4.63 (6)	$^1\text{E}, \dots 4\text{e}^4 3\text{a}_1^2 2\text{b}_1^2 5\text{e}^4 2\text{a}_2^2 4\text{a}_1^2 4\text{b}_2^2 6\text{e}^3 3\text{b}_1^1$	4.24	4.23	4.55
C	4.72 (6)	$^1\text{A}_2, \dots 4\text{e}^4 3\text{a}_1^2 2\text{b}_1^2 5\text{e}^4 2\text{a}_2^2 4\text{a}_1^2 4\text{b}_1^2 6\text{e}^4 3\text{b}_1^1$	4.28	4.28	4.71
D	6.00 (6)	$^3\text{A}_2, \dots 4\text{e}^4 3\text{a}_1^2 2\text{b}_1^2 5\text{e}^4 2\text{a}_2^2 4\text{a}_1^2 4\text{b}_1^2 6\text{e}^4 3\text{b}_1^1$	4.52	4.27	e
E	6.20 (6)	$^3\text{B}_1, \dots 4\text{e}^4 3\text{a}_1^2 2\text{b}_1^2 5\text{e}^4 2\text{a}_2^2 4\text{a}_1^2 4\text{b}_2^2 6\text{e}^4 3\text{b}_1^1$	5.63	e	e
		$^1\text{B}_1, \dots 4\text{e}^4 3\text{a}_1^2 2\text{b}_1^2 5\text{e}^4 2\text{a}_2^2 4\text{a}_1^2 4\text{b}_2^2 6\text{e}^4 3\text{b}_1^1$	5.67	e	6.00
		$^3\text{E}, \dots 4\text{e}^4 3\text{a}_1^2 2\text{b}_1^2 5\text{e}^4 2\text{a}_2^2 4\text{a}_1^2 4\text{b}_2^2 6\text{e}^4 3\text{b}_1^1$	6.02	e	e
		$^1\text{E}, \dots 4\text{e}^4 3\text{a}_1^2 2\text{b}_1^2 5\text{e}^4 2\text{a}_2^2 4\text{a}_1^2 4\text{b}_2^2 6\text{e}^4 3\text{b}_1^1$	6.03	e	e
		$^3\text{E}, \dots 4\text{e}^4 3\text{a}_1^2 2\text{b}_1^2 5\text{e}^4 2\text{a}_2^2 4\text{a}_1^2 4\text{b}_2^2 6\text{e}^4 3\text{b}_1^1$	6.08	e	e

^a Numbers in parentheses represent the uncertainty in the last digit.

^b VDEs were calculated using Δ SCF method at B3LYP/SDD level of theory.

^c VDEs were calculated using Δ SCF method at B3LYP/Ti/aug-cc-pVTZ/Au/aug-cc-pVTZ-pp level of theory.

^d VDEs were calculated using Δ SCF-TDDFT method at B3LYP/Ti/aug-cc-pVTZ/Au/aug-cc-pVTZ-pp level of theory.

^e The VDEs cannot be obtained at this level of theory.

'a' at 2.3 eV, which corresponds to detachment of Au^- . Similar thermionic emissions from superhot anions are observed even more prominently in the 355 nm spectrum (Figure 1a), where the Au^- signal is also more visible. The very weak continuous signals in the low binding energy side below the detachment threshold are likely due to the detachment of the superhot anions upon absorption of a second photon. We confirmed the thermionic and two-photon processes by varying the photon fluxes. Both the Au^- and the continuous thermionic signals were reduced at lower detachment laser fluxes. Even though the X band at 355 nm is broadened due to the thermionic emission, the onset is quite sharp, which allowed us to estimate the adiabatic detachment energy (ADE). Since vibrational structures are not resolved, the ADE is measured by drawing a straight line along the leading edge of band X in the 355 nm spectrum and then adding the spectral resolution to the intersection with the binding energy axis. The ADE obtained is 2.80 ± 0.05 eV, which corresponds to the electron affinity of TiAu_4^- .

3.2. Theoretical results

The optimized global minimum and low-lying structures of TiAu_4^- and TiAu_4 are depicted in Figure 2, along with their relative energies and point group symmetries. All cluster structures presented were obtained initially via the CK structural searches and subsequently reoptimized at the B3LYP/SDD and PBEPBE/SDD levels of theory. The calculations at both levels give a slight distorted tetrahedral structure, isomer 1 (D_{2d} , $^2\text{B}_1$) in Figure 2a, as the global minimum structure for TiAu_4^- . The four Ti–Au bonds have the same bond length of 2.54 Å at B3LYP and 2.50 Å at PBE. The two different $\angle\text{Au}–\text{Ti}–\text{Au}$ bond angles in the D_{2d} TiAu_4^- are essentially the same at the two levels of theory: 114.4° and 99.9° at B3LYP and 114.5° and 99.8° at PBE. The nearest low-lying isomer 2 (C_{2v} ,

$^2\text{A}_1$) lies 15.79 kcal/mol (B3LYP) and 18.53 kcal/mol (PBE) above the ground state. Isomer 2 is a planar triangular structure with a Au_2 unit, which can be denoted as $(\eta^1\text{Au}_2)\text{TiAu}_2^-$. All other structures are at least 40 kcal/mol above the global minimum at both levels of theory.

Neutral TiAu_4 is found to be tetrahedral with T_d symmetry and a closed-shell electronic state (structure 5 in Figure 2b). The calculated Au–Ti bond distance is 2.43 (B3LYP) and 2.40 Å (PBE), significantly reduced relative to those in the anion. Our results on TiAu_4 are consistent with the previous work [5]. The nearest low-lying isomer, 6 (C_s , $^1\text{A}'$), is similar to isomer 2 for the anion, but it is non-planar with C_s symmetry because the Au–Au–Ti unit is slightly bent. Isomer 6 is 34.22 kcal/mol (B3LYP) and 38.21 kcal/mol (PBE) higher than the global minimum T_d structure 5.

3.3. Comparison between experiment and theory

Our calculations show that the global minimum isomer 1 (D_{2d} , $^2\text{B}_1$) of TiAu_4^- is significantly more stable than the nearest low-lying isomer (structure 2 in Figure 2a). Thus, we can rule out contributions of the low-lying isomers to the experimental spectra. The computed VDEs for all the detachment channels for the global minimum structure are given in Table 1 and the simulated spectrum is shown in Figure 1d.

The global minimum structure of TiAu_4^- has a doublet ground electronic state ($^2\text{B}_1$) with a valence electron configuration of $\dots 2\text{a}_2^2 4\text{a}_1^2 4\text{b}_2^2 6\text{e}^4 3\text{b}_1^1$. All the occupied valence molecular orbitals (MOs) of TiAu_4^- are shown in Figure 3. The first detachment channel corresponds to the electron removal of the singly occupied molecular orbital (SOMO, 3b_1) to produce the singlet neutral ground state ($^1\text{A}_1$). The calculated VDE of this detachment channel is 3.16 eV at B3LYP/SDD level of theory. It is worth noting that the

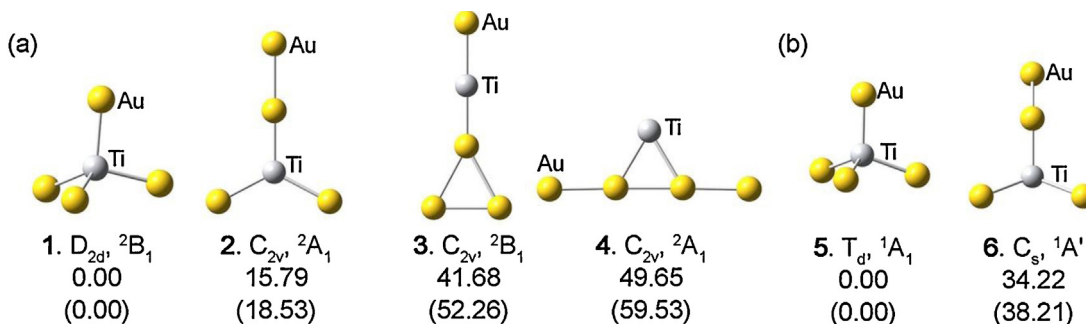


Figure 2. Optimized global minimum structure and low-lying isomers of (a) TiAu_4^- and (b) TiAu_4 . Relative energies for the isomers are given in kcal/mol at B3LYP/SDD and PBEPBE/SDD (in parentheses) levels of theory. All the relative energies have been corrected for zero-point energies.

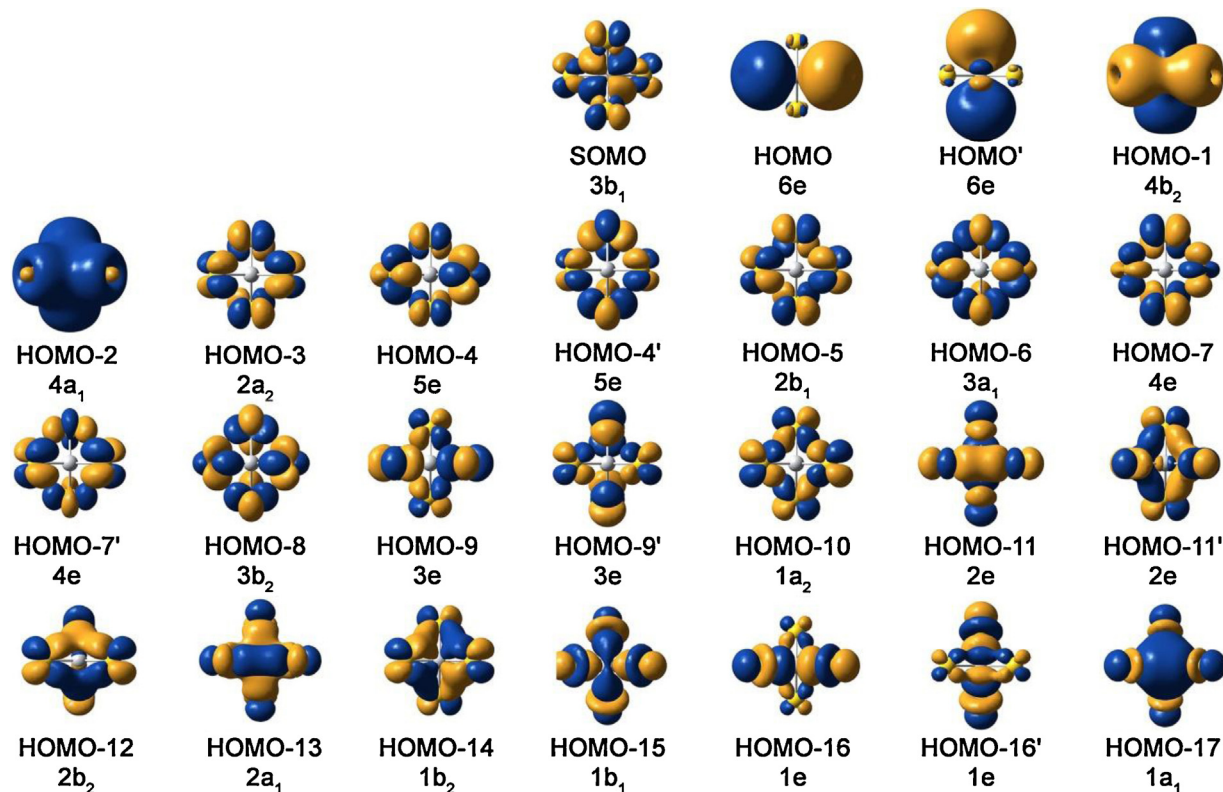


Figure 3. Counter plots of the occupied valence molecular orbitals of the ground state of the D_{2d} $TiAu_4^-$ calculated at B3LYP/SDD level of theory.

0.25 eV difference between the experiment and calculated first VDE is within the error of the computational method used. The application of larger basis set (Ti/Aug-cc-pVTZ/Au/Aug-cc-pVTZ-pp) yields a smaller VDE of 3.02 eV. Both VDEs are in good agreement with the experimental value of 2.91 eV. The calculate ADEs, based on the energy difference between the total energies of the ground state of the anion (D_{2d} , 2B_1) and that of the neutral (T_d , 1A_1), are 2.91 eV at the B3LYP/SDD level of theory and 2.78 eV using larger basis set, which also agree well with the experimental ADE of 2.80 eV. The $3b_1$ SOMO of $TiAu_4^-$ (Figure 3) involves antibonding interactions between the Au 5d and Ti 3d orbitals, consistent with the large Au–Ti bond length reduction upon electron detachment to form neutral $TiAu_4$ in its ground state. Hence, the Au–Ti breathing mode should be active in the X band, which was calculated to have a frequency of 116 cm^{-1} . Because of the symmetry change from D_{2d} to T_d upon electron detachment, the bending mode of $TiAu_4$ should also be active in the X band, which has a calculated vibrational frequency of 26 cm^{-1} . Thus, the X band should contain extensive vibrational structures of the two modes, consistent with the relatively broad width in the experimental spectra (Figure 1).

It can been seen from Table 1 that increasing the basis set produces slightly smaller VDEs and the ΔSCF method seems to under estimated the VDE values comparing to the ΔSCF -TDDFT method. However, due to the lack of several excited states in the ΔSCF -B3LYP/Ti/Aug-cc-pVTZ/Au/Aug-cc-pVTZ-pp and ΔSCF -TDDFT-B3LYP/Ti/Aug-cc-pVTZ/Au/Aug-cc-pVTZ-pp, all the following discussion are based on the ΔSCF -B3LYP/SDD method. Electron detachment from the doubly degenerate HOMO (6e) reaches the first triplet excited state (3E) with a calculated VDE of 4.21 eV, in agreement with band A at 4.42 eV. The calculated 3E – 1A_1 VDE difference of 1.05 eV is smaller than the observed X–A energy gap of 1.5 eV. The singlet final state (1E) from detachment of the 6e HOMO gives the calculated VDE of 4.24 eV. The third detachment

channel occurs from HOMO-1 ($4b_2$) reaching the 3A_1 final state that produce the 1A_2 final state with the calculated VDE of 4.28 eV. These two detachment channels are calculated at 4.55 eV and 4.71 eV using the ΔSCF -TDDFT method. They are assigned to the intense band B at 4.63 eV. The corresponding triplet final state from HOMO-1 has a calculated VDE of 4.52 eV, which agrees with band C at 4.72 eV. Following a large energy gap, the next detachment channel occurs from HOMO-2 ($4a_1$). The computed VDEs for the triple and singlet final states are 5.63 and 5.67 eV, which are in very good agreement with bands D. Three more detachment channels are calculated at 6.02 eV, 6.03 eV and 6.08 eV, which are assigned to the feature E. Hence, the broad signal between bands C and D (labeled with * in Figure 1c) cannot be due to direct one-electron processes. Following another small energy gap, all higher detachment channels involve the congested Au 5d orbitals (Figure 3 and Table 1), which are beyond the current photon energy at 193 nm. The calculated VDEs are fitted with 0.12 eV FWHM Gaussian functions to produce a simulated spectrum, as shown in Figure 1d. Overall, the simulated spectral pattern is in excellent agreement with the experimental spectrum, lending strong support for the D_{2d} global minimum of $TiAu_4^-$.

3.4. The chemical bonding in $TiAu_4$

The molecular orbitals of the T_d $TiAu_4$ are shown in Figure 4. They are similar to those of the anions (Figure 3), except that the neutral has high symmetry and higher degeneracy. It is important to point out that the LUMO of $TiAu_4$ is doubly degenerate (3e). The occupation of this orbital in the $TiAu_4^-$ anion induces Jahn–Teller distortions, resulting in the D_{2d} global minimum of anionic $TiAu_4^-$. The HOMO (4t₂) and HOMO-1 (2a₁) of $TiAu_4$ describe bonding interactions between the Au 6s and the Ti 4s orbitals, whereas HOMO-8 (1t₂) and HOMO-9 (1a₁) shown significant bonding

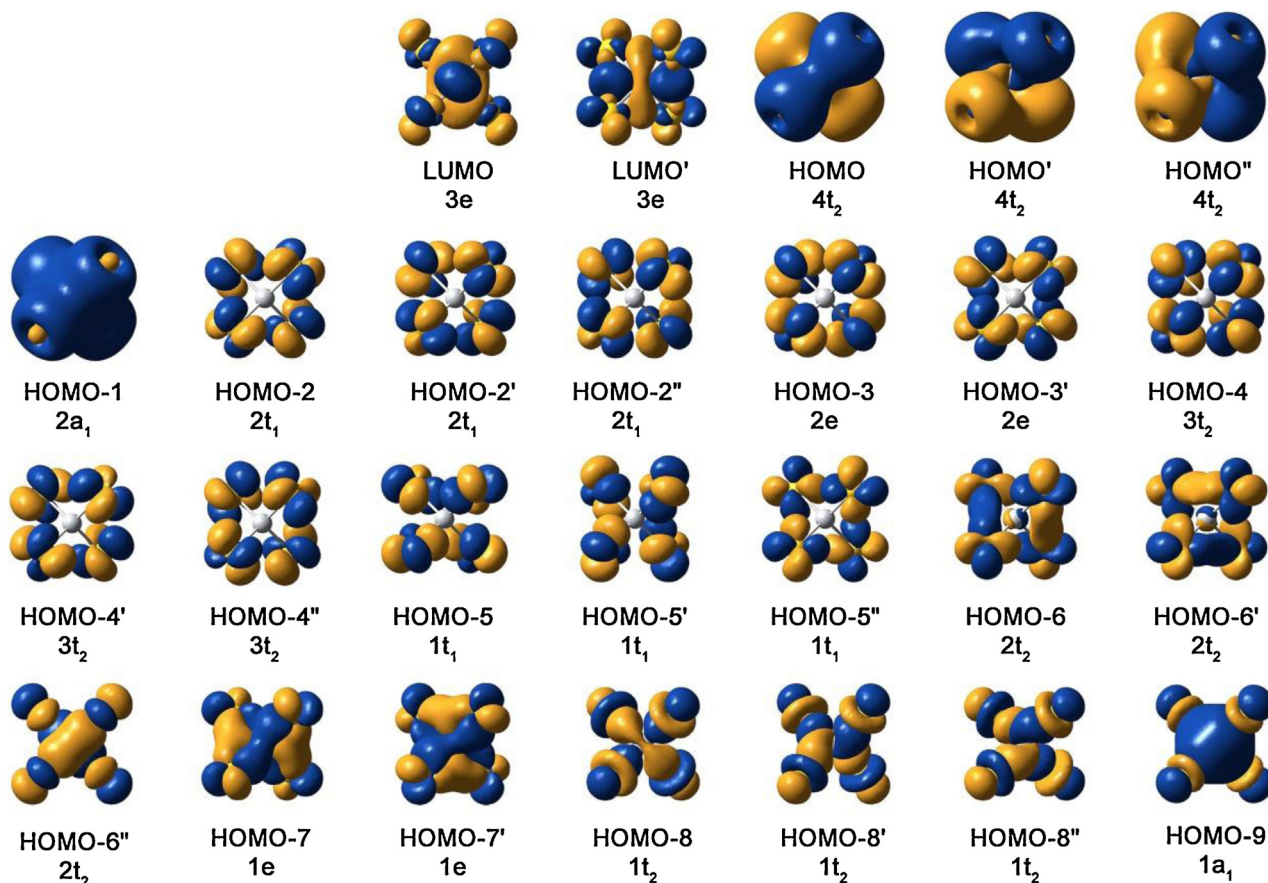


Figure 4. Counter plots of the valence orbitals of the ground state of the T_d $TiAu_4$ calculated at B3LYP/SDD level of theory.

Table 2

Comparison of the bond lengths, natural charges, and Wiberg bond indices of a series of titanium tetrahedral compound, TiX_4 ($X=H, F, Cl, Br, I$, and Au), at the B3LYP/SDD level of theory.

	Covalent radius (X) (pm)	Electro-negativity (X)	Bond length (Å)	Natural charge ($ e $)		Wiberg bond indices	
				Ti	X	Ti– X	X – X
TiH_4	31 ± 5	2.20	1.69	0.82	-0.21	0.96	0.00
TiF_4	64	3.98	1.75	1.68	-0.42	0.98	0.02
$TiCl_4$	102 ± 4	3.16	2.19	0.09	-0.02	1.49	0.05
$TiBr_4$	120 ± 3	2.96	2.34	-0.36	0.09	1.60	0.06
TiI_4	139 ± 3	2.66	2.56	-0.99	0.25	1.76	0.07
$TiAu_4$	136 ± 6	2.54	2.43	-0.24	0.06	1.37	0.05

interactions between the Au $5d_z^2$ and the Ti $3d$ orbitals. These favorable bonding interactions underlie the high stability of $TiAu_4$ and suggest that the Au – Ti bonds have multiple bonding characters.

To further understand the chemical bonding in $TiAu_4$, we performed NBO analyses based on the optimized structure at B3LYP and compared it with other known tetrahedral titanium compounds, TiX_4 ($X=H, F, Cl, Br, I$, and Au) at the same level of theory. All the bond lengths, natural charges, and Wiberg bond indices for TiX_4 ($X=H, F, Cl, Br, I$, and Au) are summarized in Table 2. In TiH_4 , Ti carries $+0.82 |e|$ residual charge and H carries $-0.21 |e|$ charge, consistent with the relatively small electronegativity of Ti (1.54) compared to that of H (2.20). The Ti atom becomes even more positively charged in TiF_4 due to the extremely large electronegativity of F . Thus, the Ti – H and Ti – F bonds have strong ionic characters. Although Br , I , and Au have larger electronegativity than Ti , the NBO analyses show that Ti carries negative charges in TiX_4 for $X=Br, I$, Au . In addition, the Wiberg bond indices [49] reveal that the Ti – H and Ti – F bonds are single bonds, but the bond order between Au

and the heavier halogens is ~ 1.5 , suggesting multiple bond characters as a result of back donations from the ligands to Ti . The negative charge on Ti in these systems is also a consequence of the back donation. The multiple bond character in $TiAu_4$ is consistent with the MO analyses mentioned above. Hence, on the bases of the NBO analyses, Au atoms behave more like heavy halogens in $TiAu_4$, as initially suggested in ref. 5. This is mainly due to the back donation of Au $5d$ to Ti $3d$. There is no such d–d interactions when Au bonds to Si or B , where it behaves more like a H atom in Si – Au or B – Au binary clusters [8,13].

4. Conclusions

In conclusion, photoelectron spectroscopy is combined with density functional theory calculations to investigate the electronic structure and bonding properties in titanium tetraauride. The electron affinity of $TiAu_4$ is measured to be 2.80 ± 0.05 eV. Photo-electron spectra of $TiAu_4^-$ reveal a large HOMO-LUMO gap for $TiAu_4$, suggesting it is a highly stable species. DFT calculations are

performed to search for the lowest energy structures for both the anion and neutral. We find that the global minimum structure of TiAu_4^- has D_{2d} symmetry, whereas neutral TiAu_4 has perfect T_d symmetry. The reduced symmetry of the anion is due to the Jahn-Teller effect because the LUMO of TiAu_4 is doubly degenerate. The global minimum structure of TiAu_4^- is confirmed by comparison of the calculated VDEs with experimental PES data. Natural bond order and molecular orbital analyses show multiple bond characters between Au and Ti in TiAu_4 due to back donation of Au 5d to Ti 3d. The bonding in TiAu_4 is found to be similar to heavy titanium tetrahalogens.

Acknowledgements

The research was supported by the National Science Foundation (CHE-1049717). Y.E. would like to thank the Scientific and Technological Research Council of Turkey (TUBITAK) for an International Postdoctoral Research Fellowship (Program 2219). The authors would like to thank Zachary A. Piazza for the discussion of the calculation.

References

- [1] P. Pyykko, Chem. Rev. 88 (1988) 563.
- [2] P. Pyykko, Angew. Chem. Int. Ed. 41 (2002) 3573.
- [3] A. Laguna, *Modern Supramolecular Gold Chemistry: Gold-Metal Interactions and Applications*, Wiley WCH, Weinheim, Germany, 2008.
- [4] L.S. Wang, Phys. Chem. Chem. Phys. 12 (2010) 8694.
- [5] L. Gagliardi, J. Am. Chem. Soc. 125 (2003) 7504.
- [6] C.S. Wannere, et al., J. Am. Chem. Soc. 127 (2005) 5701.
- [7] M. Jansen, A.V. Murding, *Gold Progress in Chemistry, Biochemistry and Technology*, Wiley, New York, 1999.
- [8] B. Kiran, X. Li, H.J. Zhai, L.F. Cui, L.S. Wang, Angew. Chem. Int. Ed. 43 (2004) 2125.
- [9] H.J. Zhai, L.S. Wang, D.Y. Zubarev, A.I. Boldyrev, J. Phys. Chem. A 110 (2006) 1689.
- [10] X. Li, B. Kiran, L.S. Wang, J. Phys. Chem. A 109 (2005) 4366.
- [11] B. Kiran, X. Li, H.J. Zhai, L.S. Wang, J. Chem. Phys. 125 (2006) 133204.
- [12] D.Y. Zubarev, A.I. Boldyrev, J. Li, H.J. Zhai, L.S. Wang, J. Phys. Chem. A 111 (2007) 1648.
- [13] H.J. Zhai, C.Q. Miao, S.D. Li, L.S. Wang, J. Phys. Chem. A 114 (2010) 12155.
- [14] W.L. Li, C. Romanescu, T. Jian, L.S. Wang, J. Am. Chem. Soc. 134 (2012) 13228.
- [15] P. Pyykko, N. Runneberg, Angew. Chem. Int. Ed. 41 (2002) 2174.
- [16] X. Li, B. Kiran, J. Li, H.J. Zhai, L.S. Wang, Angew. Chem. Int. Ed. 41 (2002) 4786.
- [17] H.J. Zhai, J. Li, L.S. Wang, J. Chem. Phys. 121 (2004) 8369.
- [18] H. Tanaka, S. Neukermans, E. Janssens, R.E. Silverans, P. Lievens, J. Chem. Phys. 119 (2003) 7115.
- [19] H. Tanaka, S. Neukermans, E. Janssens, R.E. Silverans, P. Lievens, J. Am. Chem. Soc. 125 (2003) 2862.
- [20] R. Pal, L.M. Wang, W. Huang, L.S. Wang, X.C. Zeng, J. Am. Chem. Soc. 131 (2009) 3396.
- [21] X. Li, B. Kiran, L.F. Cui, L.S. Wang, Phys. Rev. Lett. 95 (2005) 253401.
- [22] S. Zorriastain, K. Joshi, D.G. Kanhere, J. Chem. Phys. 128 (2008) 184314.
- [23] J. Long, Y.X. Qiu, X.Y. Chen, S.G. Wang, J. Phys. Chem. C 112 (2008) 12646.
- [24] J. Sui, X.Q. Wang, P.L. An, Comput. Theor. Chem. 1028 (2014) 98.
- [25] D. Dong, Z.B. Xia, W. Hui, D. Quan, Comput. Theor. Chem. 1025 (2013) 67.
- [26] C. Majumder, S.K. Kulshreshtha, Phys. Rev. B73 (2006) 155427.
- [27] M. Walter, H. Hakkinen, Phys. Chem. Chem. Phys. 8 (2006) 5407.
- [28] Q. Sun, Q. Wang, G. Chen, P. Jena, J. Chem. Phys. 127 (2007) 214706.
- [29] C. Majumder, A.K. Kandalam, P. Jena, Phys. Rev. B74 (2006) 205437.
- [30] L.M. Wang, et al., J. Am. Chem. Soc. 129 (2007) 15136.
- [31] W. Fa, J.M. Dong, J. Chem. Phys. 128 (2008) 144307.
- [32] L.F. Cui, Y.C. Lin, D. Sundholm, L.S. Wang, J. Phys. Chem. A 111 (2007) 7555.
- [33] C. Majumder, Phys. Rev. B75 (2007) 235409.
- [34] L.S. Wang, H.S. Cheng, J. Fan, J. Chem. Phys. 102 (1995) 9480.
- [35] W. Huang, L.S. Wang, Phys. Rev. Lett. 102 (2009) 153401.
- [36] A.P. Sergeeva, B.B. Averkiev, H.J. Zhai, A.I. Boldyrev, L.S. Wang, J. Chem. Phys. 134 (2011) 224304.
- [37] P.J. Hay, W.R. Wadt, J. Chem. Phys. 82 (1985) 299.
- [38] J.P. Perdew, K. Burke, M. Ernzerhof, Phys. Rev. Lett. 77 (1996) 3865.
- [39] J. Li, X. Li, H.J. Zhai, L.S. Wang, Science 299 (2003) 864.
- [40] C. Romanescu, T.R. Galeev, W.L. Li, A.I. Boldyrev, L.S. Wang, Angew. Chem. Int. Ed. 50 (2011) 9334.
- [41] T.R. Galeev, C. Romanescu, W.L. Li, L.S. Wang, A.I. Boldyrev, Angew. Chem. Int. Ed. 51 (2012) 2101.
- [42] K.A. Peterson, C. Puzzarini, Theor. Chem. Acc. 114 (2005) 283.
- [43] N.B. Balabanov, K.A. Peterson, J. Chem. Phys. 123 (2005) 064107.
- [44] F. Weinhold, C.R. Landis, *Valeency and Bonding: A Natural Bond Orbital Donor-Acceptor Perspective*, Cambridge University Press, Cambridge, UK, 2005.
- [45] M.J. Frisch, et al., *GAUSSIAN 09*, Revision A. 2, Gaussian, Inc., Wallingford, CT, 2009.
- [46] X.B. Wang, C.F. Ding, L.S. Wang, J. Chem. Phys. 110 (1999) 8217.
- [47] L.S. Wang, J. Conceicao, C. Jin, R.E. Smalley, Chem. Phys. Lett. 182 (1991) 5.
- [48] W. Weidele, et al., Chem. Phys. Lett. 237 (1995) 425.
- [49] A.E. Reed, L.A. Curtiss, F. Weinhold, Chem. Rev. 88 (1988) 899.